



Universiteit
Leiden
The Netherlands

On transport properties of Weyl semimetals

Baireuther, P.S.

Citation

Baireuther, P. S. (2017, April 26). *On transport properties of Weyl semimetals*. Retrieved from <https://hdl.handle.net/1887/48876>

Version: Not Applicable (or Unknown)

License: [Licence agreement concerning inclusion of doctoral thesis in the Institutional Repository of the University of Leiden](#)

Downloaded from: <https://hdl.handle.net/1887/48876>

Note: To cite this publication please use the final published version (if applicable).

Cover Page



Universiteit Leiden



The handle <http://hdl.handle.net/1887/48876> holds various files of this Leiden University dissertation

Author: Baireuther, P.S.

Title: On transport properties of Weyl semimetals

Issue Date: 2017-04-26

1 Introduction

1.1 Preface

Band theory is one of the most powerful quantum mechanical tools available to understand the electronic properties of crystalline solids. It has been extremely successful in grouping a wide variety of materials into just two categories: metals and insulators. In a metal, the Fermi energy lies within a band, called the conduction band. A metal is characterized by its finite conductivity at zero temperature. In an insulator, the Fermi energy lies in a gap between a fully occupied valence band and an empty conduction band. At zero temperature, the conductivity of an insulator is zero.

The finite band gap at the Fermi energy of insulators allows us to adiabatically transform different Hamiltonians with the same symmetries into one another while remaining in the ground state. However, this is not always possible. There are Hamiltonians of insulators that cannot be transformed into each other without closing the bulk gap, despite them having the same symmetries. Such insulators are topologically distinct [1].

In mathematics topology is a way to distinguish objects that cannot be transformed into each other without tearing or cutting them. For example, consider two-dimensional surfaces. If the number of holes ('genus') in two such surfaces is not the same, they can not be transformed into one another continuously. The surface of a sphere is topologically equivalent to the surface of a vase, but not to the surface of a pipe, which is in turn equivalent to the surface of a coffee mug.

In the context of topological insulators one can identify so-called topological invariants, which are integer numbers, very much like the genus of a surface. While the genus is related to the numbers of holes in the surface, the topological invariants are related to the number of topologically protected edge states at the interface of two topologically distinct insulators. These edge states are robust to weak disorder [2–4] and cannot be gapped, as long as the perturbations do not break the symmetries of the system or close the insulating bulk gap.

During the last decade, topological insulators have been in the center of attention of condensed matter research [5–9]. This thesis is concerned

1 Introduction

with a new class of topological materials, that has emerged very recently: Topological semimetals [10–18].

Semimetals are in-between metals and insulators. In semimetals, the bottom of the conduction band overlaps with the top of the valence band. Therefore, they have a gapless spectrum, which forbids adiabatic transformations. At first sight, it is therefore counterintuitive that a semimetal can have topological properties. If translation symmetry is preserved, however, we can look at the semimetal in reciprocal space. A key distinction to a normal metal is that the Fermi surface is very small. In a topological semimetal the Fermi surface shrinks all the way to a point.

Although the topological semimetal is not fully gapped, it is possible to construct planes in the Brillouin zone in which the spectrum is gapped. These planes are characterized by topological invariants [8, 19], much like the topological insulators. The bulk-boundary correspondence then implies that there exist topologically protected surface states [10]. In contrast to topological insulators, in a topological semimetal these states are only defined in parts of the Brillouin zone — they merge with the bulk bands near the gapless regions.

The focus in this thesis is on a particular topological semimetal called a *Weyl semimetal* [18, 20–22]. At first sight, a Weyl semimetal is just a three-dimensional version of graphene. However, the third spatial dimension plays a subtle, but powerful role, that distinguishes Weyl semimetals from graphene. Unlike in graphene, the existence and stability of the gapless points in the spectrum (so-called Weyl points) is not guaranteed by a symmetry, but by the third spatial dimension itself. The Weyl points are protected by a topological invariant (the so-called chirality or Berry flux) and cannot be removed by local perturbations. The only way to open a gap is to merge two Weyl points of opposite chirality. The chirality of the Weyl points leads to remarkable electronic properties, such as chiral Landau levels and the chiral magnetic effect. These, and other properties that distinguish Weyl semimetals from graphene, are the core subjects of this thesis.

1.2 Weyl semimetals

1.2.1 Band structure

Just like in graphene, the low-energy spectrum of a Weyl semimetal has a linear energy-momentum relation. The low-energy excitations are massless and move with an energy-independent velocity (analogous to the speed

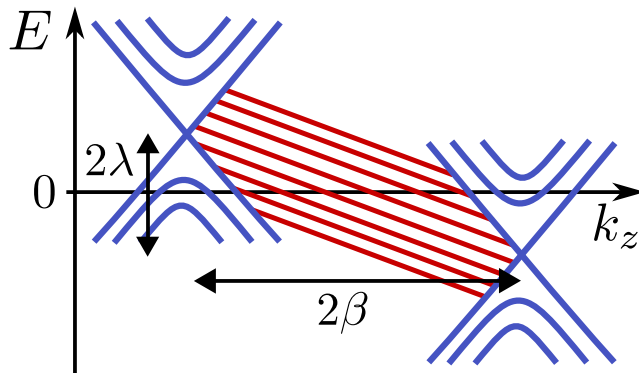


Figure 1.1: Schematic drawing of the energy-momentum relation of a Weyl semimetal slab. The bulk Weyl cones (blue) are separated in momentum space by a time-reversal-symmetry breaking magnetization β . If inversion symmetry is broken ($\lambda \neq 0$), the Weyl points are displaced with respect to each other in energy. On the surface the projection of the Weyl cones are connected by chiral edge states (red).

of light for photons). Many of the remarkable electronic properties of graphene, such as Klein tunneling [23–25], are therefore also present in Weyl semimetals. If we consider a slab geometry, which is finite in one direction and translationally invariant in the other two directions, the surface states look just like the dispersionless surface states of graphene with a zigzag edge. A schematic drawing of the band structure is shown in Fig. 1.1. In our numerical simulations, we use a tight-binding model

$$\begin{aligned}
 \mathcal{H}(\mathbf{k}) &= \tau_z(t'\sigma_x \sin k_x + t'\sigma_y \sin k_y + t'_z\sigma_z \sin k_z) \\
 &\quad + m(\mathbf{k})\tau_x\sigma_0 + \beta\tau_0\sigma_z + \lambda\tau_z\sigma_0 \\
 m(\mathbf{k}) &= m_0 + t(2 - \cos k_x - \cos k_y) + t_z(1 - \cos k_z), \quad (1.1)
 \end{aligned}$$

which is equivalent to the model introduced in [26], up to a unitary transformation. The Pauli matrices σ and τ represent spin and orbital degrees of freedom. (For brevity, we will set $\hbar \equiv 1$, and often also the lattice constant $a \equiv 1$.) The first two terms in Eq. 1.1 describe a Weyl semimetal with eight Weyl cones located at $\mathbf{k} = (\{0, \pi\}, \{0, \pi\}, \pm\beta)$ for small β . The third term, the “mass term” $\mu(\mathbf{k})$, gaps the Weyl points at $k_x = \pi$ and $k_y = \pi$ so that only two Weyl points remain at $\mathbf{k} = (0, 0, \pm\beta)$. The inversion breaking term b_0 shifts the Weyl cones in energy in opposite directions.

1.2.2 Topological properties

To understand the topological properties of a Weyl semimetal, we first focus on a single, non-degenerate Weyl cone. Such a Weyl-cone consists of a conduction band and a valence band, that *accidentally* touch at single point, the Weyl point. The Hamiltonian of a single isotropic Weyl cone reads

$$H = \chi v_F (k_x \sigma_x + k_y \sigma_y + k_z \sigma_z), \quad (1.2)$$

where $\chi = \pm$ is the chirality, v_F is the Fermi velocity, k_i a momentum component, and σ_i a spin Pauli matrix. In this context, chirality means that the momentum and the spin of electrons in a given Weyl cone are (anti-)parallel.

The Weyl Hamiltonian in Eq. 1.2 looks almost like the Hamiltonian for a single Dirac cone in graphene, with the key difference that all three Pauli matrices are coupled to the momentum. Therefore, adding any additional terms to the Hamiltonian, e.g. $m\sigma_z$, only shifts the Weyl point in momentum space or energy, but does not open a gap. This is what we mean when we say that the Weyl points are topologically protected.

To understand the existence of topologically protected surface states, we need to consider a pair of Weyl points with opposite chirality. Let us assume that those Weyl points are located at $\mathbf{k}_\chi = (0, 0, \chi k_0)$. Because the band structure of a Weyl semimetal is gapless, topological invariants [1] are not well defined. However, as mentioned in the preface, if translation symmetry is conserved, we can define the three-dimensional Brillouin zone as a stack of two dimensional planes S_{k_z} , labeled by the third component of the momentum k_z . (This is called dimensional reduction [19, 27, 28].) The spectra of all planes, except for those that contain Weyl points, are gapped. We can therefore calculate their topological invariants, the so-called Chern numbers,

$$C_{k_z} = \frac{1}{2\pi} \int_{S_{k_z}} d\mathbf{k} \cdot \mathbf{B}(\mathbf{k}) \quad (1.3)$$

by integrating the Berry flux

$$\mathbf{B}(\mathbf{k}) = \nabla_{\mathbf{k}} \times i \sum_n^{\text{filled}} \langle u_n(\mathbf{k}) | \nabla_{\mathbf{k}} | u_n(\mathbf{k}) \rangle \quad (1.4)$$

over all filled bands [1], where $u_n(\mathbf{k})$ are Bloch wave functions.

By calculating the Berry flux through a sphere that encloses one of the Weyl points, we see that Weyl points are sources and sinks of Berry flux [29], depending on their chirality. The Berry flux flows from the Weyl cone

with positive chirality to the Weyl cone with negative chirality via the time-reversal invariant points. Therefore, all planes in-between* the Weyl points have a non-trivial Chern number and are topological insulators with topologically protected surface states [10]. The Chern number of the planes outside of the Weyl points is zero, and hence they do not have topological surface states. The property that Weyl points are sources and sinks of Berry flux is another way to see that they must be topologically protected: The only way to annihilate a pair of Weyl points is to merge a source with a sink.

1.2.3 Landau levels

The Landau levels of massive electrons are quantized as $E_n \sim \sqrt{n + 1/2}$. For the massless electrons in graphene the 1/2 offset is absent, and the $n = 0$ Landau level is magnetic-field independent [30]. In a three-dimensional Weyl semimetal the Landau levels also possess a dispersion along the direction of the magnetic field. The zeroth Landau level is chiral and disperses only in one direction [31].

To derive the Landau levels of a Weyl semimetal, we consider a single isotropic Weyl cone with chirality χ and include the vector potential \mathbf{A} of the magnetic field via

$$H = \chi v_F (\mathbf{k} - q\mathbf{A}) \cdot \boldsymbol{\sigma}, \quad (1.5)$$

where we will assume $q > 0$. We take the magnetic field in the z -direction and choose the symmetric gauge

$$\mathbf{A} = (-By/2, Bx/2, 0). \quad (1.6)$$

An instructive way [32–34] to calculate the spectrum of such a Hamiltonian is to introduce the canonical momenta

$$\Pi_x \equiv k_x + qBy/2 \quad \Pi_y \equiv k_y - qBx/2, \quad (1.7)$$

whose commutation relation is given by

$$[\Pi_x, \Pi_y] = iqB. \quad (1.8)$$

*“In-between” the Weyl points is defined as follows: In a Dirac semimetal, the Dirac cones are doubly degenerate. By breaking inversion or time-reversal symmetry, these cones become separated from each other in the Brillouin zone. “In-between” the Weyl points is then defined as a line in the Brillouin zone that connects the Weyl points via the Dirac point from which they emerged.

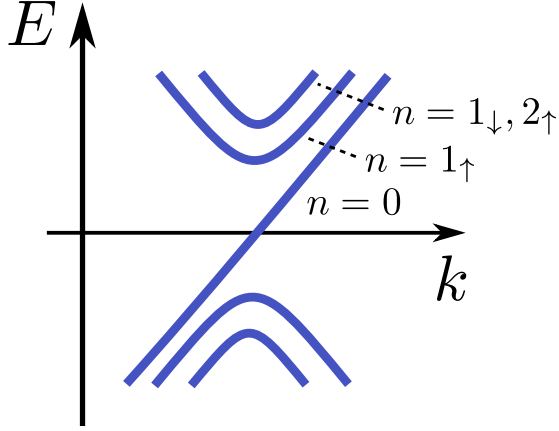


Figure 1.2: Landau levels of a single Weyl cone with positive chirality $\chi = +$.

In the z -direction, the motion is not affected by the magnetic field. In the usual way, we introduce raising and lowering operators

$$a = \sqrt{\frac{1}{2qB}}(\Pi_x + i\Pi_y), \quad a^\dagger = \sqrt{\frac{1}{2qB}}(\Pi_x - i\Pi_y), \quad (1.9)$$

which act on the Landau level index n . In this notation, the Hamiltonian reads*

$$H = \chi\sqrt{2qB}v_F(a\sigma_- + a^\dagger\sigma_+) + \chi v_F k_z \sigma_z, \quad (1.10)$$

where $\sigma_\pm = (\sigma_x \pm i\sigma_y)/2$. The zeroth Landau level ($n = 0$) is special [31], the only eigenstate is

$$H|n = 0, k_z, \uparrow\rangle = \chi v_F k_z |n = 0, k_z, \uparrow\rangle. \quad (1.11)$$

The higher Landau levels can be found by squaring the Hamiltonian

$$H^2 = qBv_F^2(2a^\dagger a + 1 - \sigma_z) + v_F^2 k_z^2. \quad (1.12)$$

From this, we can read off the $n \geq 1$ Landau levels

$$E_{n,\uparrow} = \pm v_F \sqrt{k_z^2 + 2qBn} \quad \text{and} \quad E_{n,\downarrow} = \pm v_F \sqrt{k_z^2 + 2qB(n+1)}, \quad (1.13)$$

which are illustrated in Fig. 1.2.

*We used the convention $q > 0$.

1.2.4 Chiral anomaly

The chiral anomaly is the condensed matter analogue of the Adler-Bell-Jackiw anomaly from particle physics [35, 36]. In high-energy physics, massless fermions in odd spatial dimensions have chiral symmetry. This means that the number of fermions with a given chirality, and therefore the total chiral charge, is conserved. In a Weyl semimetal, the low-energy physics is described by the same relativistic equation. However, chiral symmetry can be broken by applying a magnetic and an electric field in parallel. The electric field pumps electrons from one Weyl cone to the other, therefore changing the total chiral charge. This so-called chiral anomaly has been studied in the condensed matter context for some time [31, 37, 38].

Many of the most fascinating transport phenomena of Weyl semimetals are direct consequences of the chiral anomaly, most famously the huge magnetoconductance [31, 39–41] and the chiral magnetic effect [42–46].

1.2.5 Surface states

The surface band of a Weyl semimetal is one of its most remarkable features and a key experimental signature. The Fermi surfaces, that are formed by the intersection of the surface bands with the Fermi energy, are called Fermi arcs. They are open lines which run from one projection of a Weyl cone to another [10]. This is illustrated in Fig. 1.3 a. Usually, Fermi surfaces are closed contours, separating filled from empty states. So how can an open Fermi surface exist? The answer is that the Fermi arcs on both surfaces complement each other. Together, they form a closed Fermi surfaces [47]. If we were to make the Weyl semimetal thinner and thinner, the Fermi arcs would eventually merge into a closed Fermi surfaces.

The real-space properties of the surface states are also unusual and interesting. They are chiral, in the sense that they disperse only in one direction, circling around the direction of the internal magnetization. If inversion symmetry is broken, their velocity also has a component along the magnetization. In a cylinder geometry, where the Weyl cones are separated along the translationally invariant axis, the surface states have the shape of a solenoid and spiral along the cylinder surface as shown in Fig. 1.3 b.

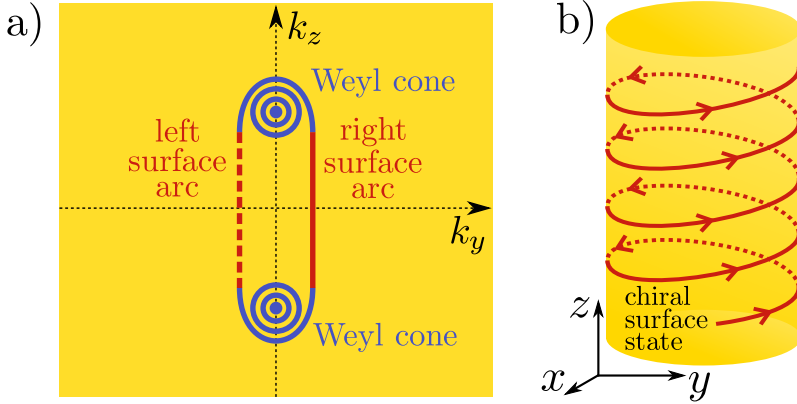


Figure 1.3: Left: Schematic illustration of the density of states of a Weyl semimetal in a slab geometry at an energy slightly away from the band touching point. The slab is finite in the x -direction with width W and translation invariant in the y - and z -directions. Due to finite size quantization, the density of states of the Weyl cones consists of several discrete circles (blue). The surface arcs (red) at the left ($x = 0$) and right ($x = W$) surface connect near the Weyl cones. Together, they form a closed contour. Right: For a cylindrical Weyl semimetal wire, the chiral surface states have the shape of a solenoid.

1.2.6 Experimental realizations

The interest in Weyl semimetals exploded with their experimental discovery in 2015. The first experimental realization was in tantalum arsenide (TaAs) [48–51]. Soon after, Weyl semimetals were reported in niobium arsenide (NbAs) [52] and tantalum phosphide (TaP) [53]. It turns out all of those materials have a very similar screw-like crystal structure. They are symmetric under a combination of rotation and translation [52, 53], a so-called non-symmorphic C_4 symmetry.

All of these pioneering experiments used a combination of low- and high-energy angle-resolved photoemission spectroscopy (ARPES). The low-energy (ultraviolet) ARPES probes the surface dispersion and shows the Fermi arcs. The high-energy (soft X-ray) ARPES probes the underlying bulk dispersion and shows the Weyl cones. One of the most impressive proofs that TaAs is indeed a Weyl semimetal is shown in Fig. 1.4. In the top part (green), a low-energy ARPES map shows the Fermi arcs on the surface. In the bottom part, the low-energy ARPES map is overlaid with a high energy ARPES map, which shows the projections of the Weyl

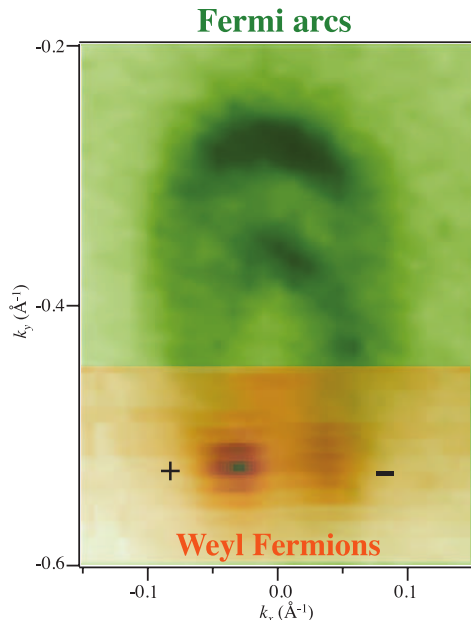


Figure 1.4: High-resolution ARPES maps of TaAs. Green region: Surface state Fermi surface map (darker color means higher ARPES signal). Brown region: Surface state Fermi surface map overlaid with bulk Fermi surface map. The surface Fermi arcs indeed terminate at the projections of the bulk Weyl points on the surface Brillouin zone. Figure from Ref. [48]. Reprinted with permission from AAAS.

points onto the surface Brillouin zone. We see that the Fermi arcs indeed terminate at projections of the Weyl points.

So far, all experimental realizations are Weyl semimetals with preserved time-reversal symmetry. However, several proposals have been put forward on how to realize Weyl semimetals with broken time-reversal symmetry [10, 54, 55]. In this thesis, we focus on the time-reversally broken situation, because it provides the minimal number of two Weyl points — when time-reversal symmetry is preserved one must have at least four Weyl points.

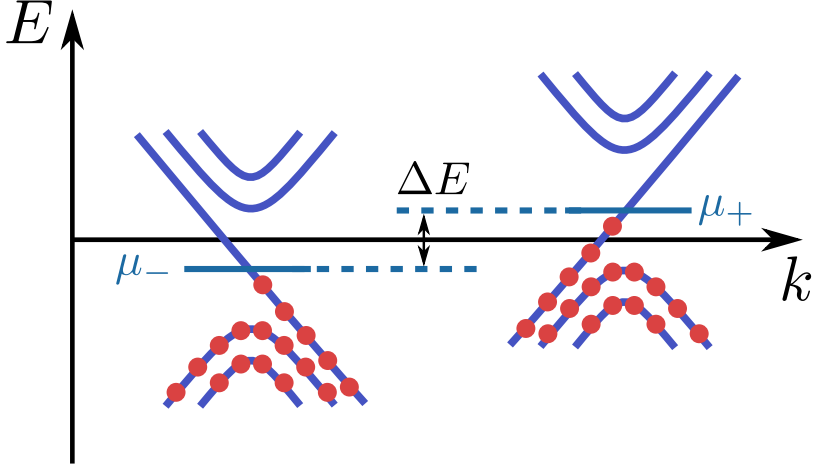


Figure 1.5: Illustration of the chiral chemical potentials μ_χ induced by an inversion breaking perturbation. The energy difference between the two Weyl points ΔE is the difference of the chiral chemical potentials.

1.3 Chiral magnetic effect

The Chiral Magnetic Effect (CME) is a “topological” current response, that is directly related to the chiral anomaly. Its universal value

$$j = (e/h)^2 \Delta E B \quad (1.14)$$

does not depend on the details of the material or model. The only terms that enter are the energy displacement of the Weyl points ΔE and the amplitude of the external magnetic field B . Initially, it was believed that the chiral magnetic effect might be a static current response. However, it is now understood that a slow periodic modulation of either ΔE or B is needed to overcome relaxation. The reason is that in any real system, there will always be a relaxation channel that scatters between the Weyl cones, even though this scattering is suppressed by the separation of the Weyl cones in the Brillouin zone. In this thesis, we therefore study the CME as a response to an oscillating parameter. The CME is one of the unique features of a Weyl semimetals that sets it apart from graphene.

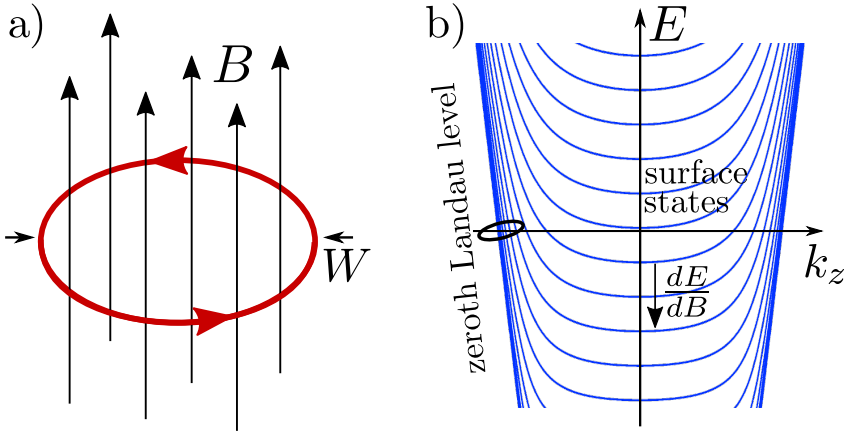


Figure 1.6: Left: In a wire geometry with diameter W , the chiral surface state encircles the entire magnetic flux. Right: Low-energy dispersion of a Weyl semimetal in a strong magnetic field. The surface states merge near the Weyl points and form the zeroth Landau levels (cf. Fig. 3.1, Chapter 3).

1.3.1 Chiral magnetic effect with Landau levels

In the first studies of the chiral magnetic effect [42–45], a Weyl semimetal was placed into a static magnetic field, strong enough for Landau levels to develop. Then, by means of an inversion symmetry breaking perturbation, the Weyl cones were periodically shifted up and down in energy in opposite directions. This so-called chiral chemical potential $\mu_\chi \approx \chi\lambda$ creates a non-equilibrium distribution at each Weyl cone, as illustrated in Fig. 1.5. The chiral Landau levels carry electron and hole currents in opposite directions. Together, they create a universal current density (Eq. 1.14).

We can derive the universal coefficient $(e/h)^2$ by very simple arguments, using an approach similar to the well-known Landauer formula, which we introduce in chapter 3. In contrast to the original Landauer formula, here the reservoirs are separated in momentum space rather than in real space. The contribution of the Weyl cone with positive chirality to the current is the product of the conductance per mode, the number of modes, and the chiral voltage μ_+/e . The conductance per mode is e^2/h and the degeneracy of the zeroth Landau level BA/Φ_0 , where \mathcal{A} is the cross section of the wire and $\Phi_0 = h/e$ is the magnetic flux quantum.

1 Introduction

Altogether, the current response is given by

$$I_+ = \frac{e^2}{h} \frac{eAB}{h} \frac{\mu_+}{e}. \quad (1.15)$$

The zeroth Landau level of the Weyl cone with negative chirality disperses in the opposite direction. At the same time, the chiral chemical potential of the other Weyl cone is the negative equal $\mu_- = -\mu_+$. Therefore, both Weyl cones contribute equally to the current, resulting in the current density 1.14.

1.3.2 Chiral magnetic effect without Landau levels

In chapter 3 we introduce a variant of the chiral magnetic effect in a weak oscillating magnetic field, that does not rely on the presence of Landau levels. For this, we consider a Weyl semimetal with both, broken time- and broken inversion symmetry. We have found that in this case the topological response is carried by the surface states. This is unexpected, because one would expect a surface current to scale with the circumference, rather than the cross section. The reason for the unusual scaling of the response is that the chiral surface states encircle the entire flux (see Fig. 1.6 a), and therefore have a magnetic moment that scales with the diameter W .

In fact, there is a deep connection between the two manifestations of the chiral magnetic effect: If one slowly turns on a strong magnetic field, the surface bands are shifted in energy and merge near the Weyl points into the zeroth Landau level (Fig. 1.6 b). Therefore, the states that carry the chiral magnetic effect in the conventional CME and our variant are directly related.

1.4 Interfaces with superconductors

1.4.1 Andreev scattering

In a superconductor, excitations consist of unpaired electrons (filled states above the Fermi level) or holes (empty states below the Fermi level). These excitations can be described in a mean-field approximation as moving in a background pair potential, which is formed by the condensate of Cooper pairs. Electrons can be scattered into holes by the pair potential, a process known as Andreev scattering [56, 57]. When an electron is converted into a hole, a Cooper pair is formed, which accounts for the missing $2e$ charge (see Fig. 1.7).

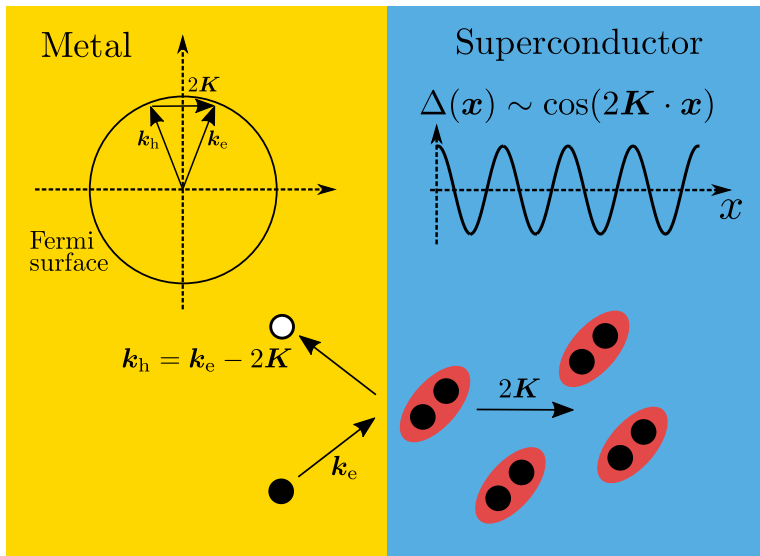


Figure 1.7: Schematic drawing of Andreev-Bragg scattering in a metal-superconductor junction. Bottom: Sketch of the Andreev scattering process. An electron enters the superconductor, where it forms a Cooper pair together with another electron. As a result, a hole is scattered back into the metal. Top left: Schematic drawing of the Brillouin zone of the metal. If the wave vector of the PDW connects two points of the Fermi surface, Andreev-Bragg scattering is allowed. Right: Drawing of the spatial dependence of the order parameter as a function of position.

Andreev scattering has a series of surprising features, that are discussed in more detail for example in [58, 59]. Most remarkably, it explains why there is a finite conductance from a metal into a superconductor at the Fermi energy, despite the excitation gap in the superconductor: An incoming electron is not simply transmitted into the superconductor, but gets Andreev reflected into a hole, transferring a charge of $2e$ from the metal into the superconductor. Therefore, the conductance from a normal metal into a superconductor (assuming an ideal interface) is twice the normal-state conductance. If the interface is not ideal, described for example by a finite transmission probability T , the conductance drops quadratically $\propto T^2$. This quadratic dependence derives from the two particle nature of Andreev scattering.

The conversion of an electron into a hole by Andreev scattering at

1 Introduction

a metal-superconductor interface introduces a phase coherence between electrons and holes in the metal. This coherence extends the properties of the superconductor into the metal. Most notably, the local density of states near the interface is suppressed around the Fermi energy. One speaks of *proximity effect* and *induced superconductivity*. The relationship between Andreev scattering and the proximity effect has been reviewed in detail in [60]. In a ballistic system, the length scale on which superconductivity is induced into the metal is the electron-hole coherence length in the metal. It is often much longer than the coherence length in the superconductor, which characterizes the “size” of Cooper pairs. This coherence is, however, rapidly destroyed if the metal breaks time-reversal symmetry. There also exists an inverse proximity effect: The pair-breaking scattering in the metal reduces the pairing amplitude in the superconductor near the interface [61].

1.4.2 Andreev-Bragg scattering

In a conventional superconductor, Cooper pairs carry zero net momentum. Therefore, momentum conservation dictates that an Andreev-reflected hole carries the same momentum as the incoming electron. Since the mass of a hole is the negative equal of the electron, in an ideal and time-reversal symmetric setting, the hole is reflected into the direction where the electron came from: $\mathbf{v}_h = \mathbf{k}_e/(-m_e) = -\mathbf{v}_e$. Its reflection angle is the opposite of that of a billiard ball bouncing from a hard wall (so-called retroreflection).

There exist also unconventional superconductors [62–65], where the Cooper pairs may carry a finite net momentum. From a theoretical perspective, the FFLO phase [66, 67] has received a lot of attention. The order parameter of such a superconductor varies periodically in space $\Delta_{2\mathbf{K}}(\mathbf{x}) \sim \cos(2\mathbf{K} \cdot \mathbf{x})$.

The interest in these so-called pair density waves has recently been revived, when it was suggested that they might play a role in the pseudogap phase of cuprate superconductors [68]. If an electron Andreev scatters from a pair density wave, the momentum of the outgoing hole is shifted: $\mathbf{k}_h = \mathbf{k}_e - 2\mathbf{K}$. If we take multiple Andreev scattering processes into account, we see that electrons, that are reflected as electrons, are shifted by even multiples of the Cooper pair momentum $\mathbf{k}'_e = \mathbf{k}_e - 2n \cdot 2\mathbf{K}$. If on the other hand an electron is scattered into a hole, the momentum is shifted by an odd multiple $\mathbf{k}_h = \mathbf{k}_e - (2n + 1) \cdot 2\mathbf{K}$. In a sense, the Cooper pairs act very much like a crystal lattice, absorbing and emitting quantized momenta.

Following this analogy, we call this type of scattering Andreev-Bragg

scattering. In general, the scattering angle in position space is determined by which points of the Fermi surface of the non-interacting system are connected by multiples of the Cooper pair momentum. In extreme cases, the scattering angle can be the opposite of conventional Andreev reflection.

1.4.3 Proximity effect in Weyl semimetals

In Weyl semimetals, the proximity effect is fundamentally different for those with and those without time-reversal symmetry. In the time-reversal symmetric case, the proximity to a spin singlet s -wave superconductor will gap the Weyl cones [69]. In Weyl semimetals with broken time-reversal symmetry, on the other hand, the proximity effect is suppressed and only affects the states that are localized at the interface between the Weyl semimetal and the superconductor. The reason is that a conventional superconductor pairs electrons from $+\mathbf{k}$ with electrons from $-\mathbf{k}$, hence from different Weyl cones. In a time-reversal symmetric Weyl semimetal, these Weyl cones have the same chirality due to Kramers degeneracy. In a Weyl semimetal with broken time-reversal symmetry, however, the cones have opposite chirality. In order for a superconductor to induce a gap, it would have to flip the chirality, which conventional spin singlet s -wave superconductors do not do.

At the interface, the situation is different. The interface states live both in the Weyl semimetal and in the superconductor. In the Weyl semimetal, they are localized by the time-reversal breaking magnetization, in the superconductor by the coherence length. Their orbital structure is therefore a hybrid of the orbital structure in the Weyl semimetal and the orbital structure in the superconductor. An interesting feature of these interface states is that the pairing is between electrons from the same band. This band splits into two, nearly charge neutral bands, which are called Majorana bands [69–71].

1.5 This thesis

In this section, we give a brief outline of the topics discussed in the chapters of this thesis.

Chapter 2

Topological insulators are classified based on their symmetries. The celebrated “ten-fold way” [28] considers time-reversal, particle-hole, and chiral

1 Introduction

symmetry. (There also exist topological insulators that do not fall into these categories.) In this chapter, we study a layered system with anti-ferromagnetic order, a so-called anti-ferromagnetic topological insulator [72]. In this system, time-reversal symmetry is broken locally, but restored in conjunction with a translation by half a unit cell. Unlike true time-reversal symmetry, this effective time-reversal symmetry is destroyed by weak disorder. However, in our studies, we find a remarkable robustness of the topological phase against electrostatic disorder. The reason is that the symmetry still holds *on average*, placing the antiferromagnetic topological insulator in the class of statistical topological insulators [73, 74].

Weyl semimetals make their first appearance in this chapter, but not yet as a stable phase — they require fine tuning of parameters. Nevertheless, we are able to calculate the conductance and the Fano factor (ratio of shot noise power and average current) at the Weyl point. Our key finding is that the Fano factor is distinct from the $1/3$ value in graphene.

Chapter 3

The chiral magnetic effect (CME) is a unique experimental signature of a Weyl semimetal that does not exist in graphene. It has been studied extensively as a response of a Weyl semimetal in a strong magnetic field to a slowly oscillating inversion breaking perturbation. However, such a perturbation is difficult to achieve experimentally. In this chapter, we study the complementary response of a Weyl semimetal with broken inversion symmetry to a small oscillating magnetic field. We find that, in this case, the CME has a surface contribution from the Fermi arc that scales with sample size in the same way as the bulk contribution. While the bulk contribution is not universal, and susceptible to disorder, we argue that the surface contribution is robust and universal, demonstrating its topological origin.

The CME from the surface Fermi arcs persists in the limit of an infinitesimally small magnetic field, when no Landau levels are formed. This “chiral magnetic effect without Landau levels” is reminiscent of the “quantum Hall effect without Landau levels”.

Chapter 4

The surface states of a Weyl semimetal with broken time-reversal and inversion symmetry form a chiral solenoid in *real space* (see Fig. 1.3). In the previous chapter 3 we showed that this solenoid carries the topological response to an oscillating magnetic field. In this chapter, we investigate

what happens if we coat the solenoid with a superconductor. We find that the proximity effect is short-ranged, affecting only the states localized at the Weyl semimetal – superconductor interface. There, the proximity effect splits the surface mode into a pair of Majorana modes. We derive an effective surface Hamiltonian and show how such a system can be used to trap Majorana fermions.

Chapter 5

In the final chapter, we depart from Weyl semimetals to study another type of system that has Fermi arcs. Spectroscopy of the pseudo-gap phase in high T_c -cuprates has revealed such disconnected pieces of Fermi surface. Even though these materials have been studied for several decades, there is no consensus about the microscopic mechanism behind the pseudo-gap phase. Recently, Patrick Lee proposed that an extreme form of finite-momentum Cooper pairing, a so-called pair density wave, might be the solution to this ongoing puzzle [68]. The pairing is called Amperian, because it is similar to the attractive force from Ampère’s law that appears between two parallel currents.

We show that Amperian pairing would lead to specular Andreev reflection (rather than the usual retroreflection) and we propose a simple three-terminal setup to detect it.

